Dynamic hardness and reduced modulus determination on the (001) face of β-Sn single crystals by a depth sensing indentation technique

2007 J. Phys.: Condens. Matter 19 306001

(http://iopscience.iop.org/0953-8984/19/30/306001)

IOP PUBLISHING JOURNAL OF PHYSICS: CONDENSED MATTER

J. Phys.: Condens. Matter **19** (2007) 306001 (17pp) doi:10.1088/0953-8984/19/30/306001

Dynamic hardness and reduced modulus determination on the (001) face of β-Sn single crystals by a depth sensing indentation technique

O Şahin[1,3], O Uzun[2], U Kölemen[2] and N Uçar[1]

[1] Department of Physics, Art and Science Faculty, Süleyman Demirel University, Isparta, Turkey
[2] Department of Physics, Art and Science Faculty, Gaziosmanpaşa University, Tokat, Turkey

E-mail: sahin@fef.sdu.edu.tr and sduosman@gmail.com

Received 20 December 2006, in final form 4 June 2007
Published 3 July 2007
Online at stacks.iop.org/JPhysCM/19/306001

Abstract

In this work, the creep behaviour of β-Sn single crystals having different growth directions under different peak indentation test loads (10, 20, 30, 40, and 50 mN) was investigated at room temperature during indentation tests. It was found that a 'nose' appears in the unloading segment of the applied indentation test load–penetration depth curve. When a 'nose' occurs, the apparent unloading stiffness S_u, defined as dP/dh, is negative and the reduced modulus can no longer be calculated from the Oliver–Pharr method (Oliver and Pharr 1992 *J. Mater. Res.* **7** 1564). The 'nose' disappears when the load hold before unload is lengthened. The correction term due to the creep is the ratio of indenter displacement rate at the end of the load hold to unloading rate (Feng and Ngan 2002 *J. Mater. Res.* **17** 660; Tang and Ngan 2003 *J. Mater. Res.* **18** 1141). Besides, the effect of creep on contact-depth measurement is considered. Removal of creep effects in both contact-area and contact stiffness measurement leads to satisfactory prediction of the dynamic hardness (H_d) and reduced modulus in β-Sn single crystals. The experimental results reveal that the measured hardness values exhibit a peak-load dependence, i.e. an indentation size effect (ISE). Such peak-load dependence is then analysed using the Meyer law, the Hays–Kendall approach, the proportional specimen resistance (PSR) model, the modified PSR (MPSR) model, and the Nix–Gao model. As a result, the modified PSR model is found to be the most effective one for H_d determination of β-Sn single crystals.

(Some figures in this article are in colour only in the electronic version)

[3] Author to whom any correspondence should be addressed.

0953-8984/07/306001+17$30.00

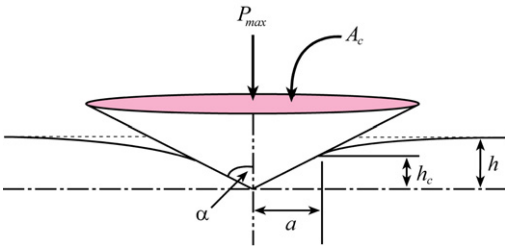

Figure 1. Conical indentation into a half space.

1. Introduction

Indentation experiments have long been used to measure the hardness of materials. Interest in the indentation test as a means of measuring elastic properties has grown recently with the development of very low-load, depth-sensing indentation (DSI) or nanoindentation instruments. These instruments have become a commonly accepted technique for measuring the surface mechanical properties of materials and allow one to make indentations as shallow as a few nanometres. One of the most widespread methods in these instruments is that proposed by Oliver and Pharr (OP) in 1992 [1]. This method has become a standard method in analysis software of commercially available nanoindenter instruments.

1.1. Oliver–Pharr (OP) method

In the OP method, it is assumed that, during the unloading process, the contact between the tip and the surface is purely elastic. In elastic modulus measurement, the contact depth, h_c, is calculated using the following equation:

$$h_c = h_{max} - \beta \frac{P_{max}}{S_u} \tag{1}$$

where h_{max} is the maximum indenter displacement at the onset of unloading, P_{max} is the load before unloading, S_u is the contact stiffness at the onset of unloading, and β is a constant depending on the indenter geometry ($\beta = 0.72$ for the Vickers tip). On the other hand, the reduced modulus, E_r, given by equation (2), can be obtained from the classical contact mechanics results [1]:

$$E_r = \frac{\sqrt{\pi}}{2} \frac{S_u}{\sqrt{A_c}} \tag{2}$$

where $A_c = f(h_c)$ is the contact area (figure 1). The area of contact at peak load is determined by the geometry of the indenter and the depth of contact, h_c.

1.2. Feng–Ngan (FN) method

Both equations (1) and (2) are based on the assumption that the tip–sample contact is purely elastic. Unfortunately, in many cases, the contact between the tip and the sample is far from purely elastic. In this situation, a creep effect during the indentation, even for metals at room temperature, can be seen. This effect has been reported by many researchers [2–5]. Such a significant creep effect at the peak load may influence the subsequent unloading behaviour, i.e., when the unloading rate is slow. In the extreme case of creep dominating elastic recovery at the onset of unload, the applied indentation test load–penetration depth curve may even exhibit

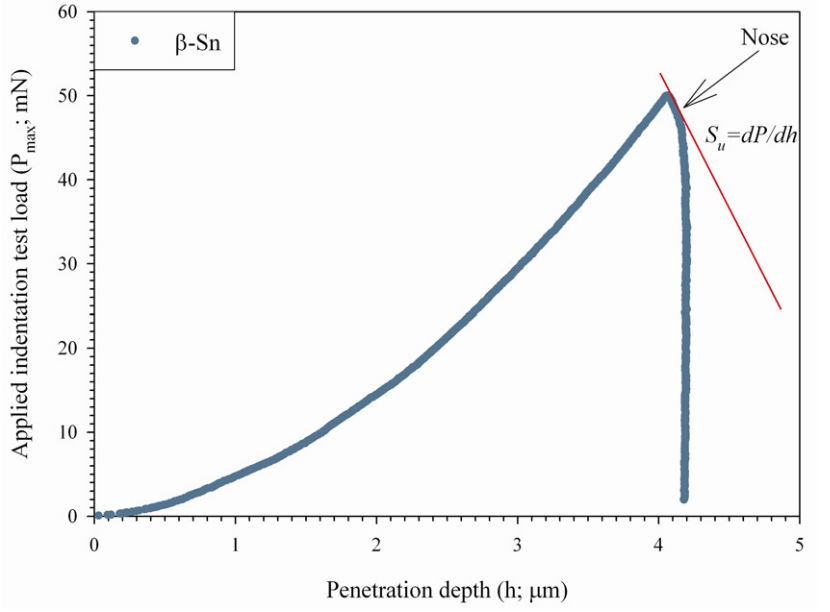

Figure 2. A situation where a nose seen in the unloading curve; the apparent unloading stiffness is negative.

a 'nose' [4, 5]. Figure 2 shows an example of the β-Sn single crystal. When a nose occurs the apparent unloading contact stiffness will be negative, but even when an obvious nose does not occur the apparent stiffness may be still a severe overestimation of the true unloading stiffness. The nose disappears when the unloading rate increased or when the load hold before unload is lengthened. In this case, the reduced modulus cannot be calculated accurately using the OP method.

In a recent investigation, Feng and Ngan [4, 6] proposed a simple method to correct for a measurement of contact stiffness ($S_u = dP/dh$). They showed, assuming linear viscoelasticity, that in an experiment involving a brief load hold prior to unloading (figure 3) the relationship between the true (elastic) unloading stiffness S_e and the observed unloading stiffness S_u is given by equation (3) [4, 6]:

$$\frac{1}{S_e} = \frac{1}{S_u} + \frac{\dot{h}_h}{|\dot{P}|}, \tag{3}$$

where the second term in equation (3) is the correction due to creep and thermal drift. $\dot{P}$ is the unloading rate at the onset of unload. Here, $\dot{h}_h$ is the indenter displacement recorded at the end of the load hold. This term can be calculated by fitting the $h(t)$ curve (t; time) like that shown in figure 4 by the following empirical law:

$$h(t) = h_i + \beta(t - t_i)^{1/3} + Kt \tag{4}$$

where h_i, β, t_i, and K are fitting constants. Feng and Ngan [4] showed that if S_e is used instead of S_u in equation (2) accurate reduced moduli can be obtained in metallic materials for Cu, Al, and Ni_3Al.

On the other hand, the dynamic hardness, H_d, is usually defined as the ratio of the applied peak indentation test load, P_{max}, to the projected contact area of the hardness impression, A_c.

$$H_d = \frac{P_{max}}{A_c} = \frac{P_{max}}{26.43h_c^2}. \tag{5}$$

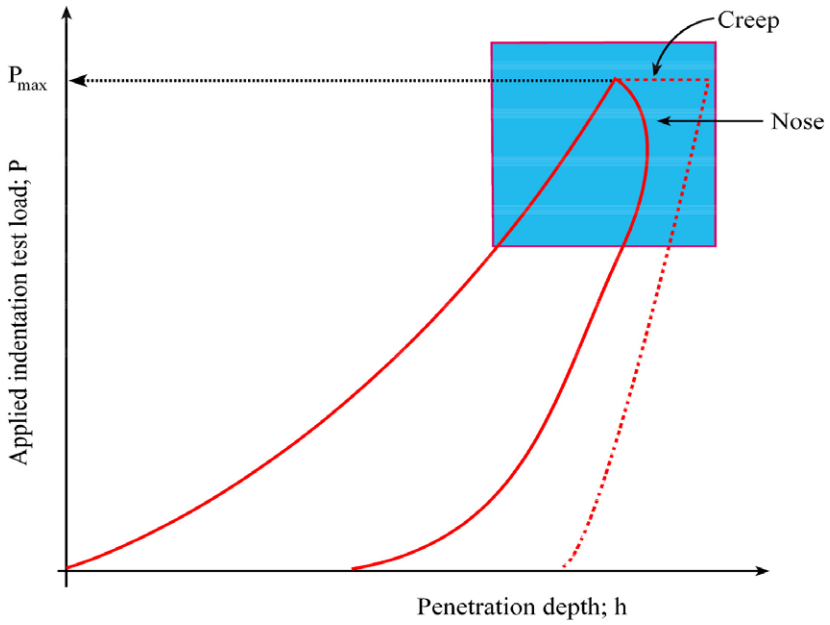

Figure 3. Removal of nose effect involving a brief load hold prior to unloading.

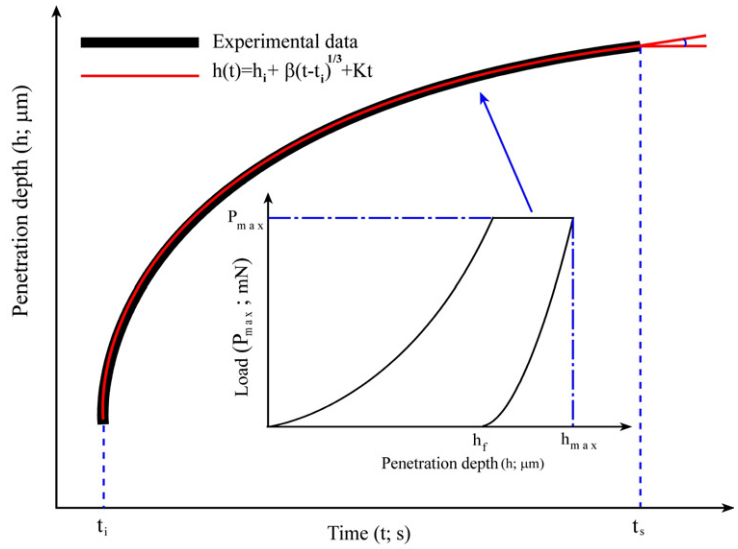

Figure 4. Penetration depth–time curve of the load-hold process.

1.3. Tang–Ngan (TN) method

Linear viscoelasticity problems are conventionally solved by the correspondence principle between elasticity and linear viscoelasticity as suggested by Radok [7]. However, for the indentation problem shown in figure 1 in which the boundary also changes with load, Lee and Radok [8] have shown that the correspondence principle can give a correct result only when

the contact size $a(t)$ at time t does not decrease. The indentation problem under a general load schedule has been solved by Ting [9], whose solution agrees with that of Lee and Radok [8] for the case of monotonically increasing $a(t)$.

Feng and Ngan [4] are interested in predicting the maximum in $a(t)$ function, i.e., the nose, and so they can legitimately use the correspondence principle to calculate the increasing portion of the $a(t)$ function up to the maximum point. Their analysis is based on nondecreasing $a(t)$. On the other hand, the Feng and Ngan procedure leaves the issue of A_c unaddressed. Tang and Ngan [10] developed a simple formula that can be used to correct for the creep effects in the contact depth h_c. Their procedure is similar to that used by Oliver and Pharr [1] in deriving equation (2); the only difference is the addition of the creep term. As a result, they found the contact depth:

$$h_c = h_{max} - \beta \frac{P_{max}}{S_u}\left(1 + S_u \frac{\dot{h}_h}{|\dot{P}|}\right) = h_{max} - \beta \frac{P_{max}}{S_e}, \tag{6}$$

where $\beta = 2(1-2/\pi)$ is the same constant as in OP's results in equation (1), and S_e is the same corrected stiffness as given by Feng and Ngan's [4, 6] results in equation (3). The correction formula for the contact depth in equation (6) derived by Tang and Ngan [10] therefore has the same form as OP's original equation (1), except that the contact stiffness has to be corrected for creep using Feng and Ngan's correction term given in equation (3).

The physical background of applied indentation test load–penetration depth behaviour of single crystals on a nanometre scale has been a matter of intensive experimental [11, 12] and theoretical study [13, 14]. On the other hand, in the literature, few studies deal with the mechanical behaviour of β-Sn single crystals via a conventional experimental procedure [15, 16]. The DSI method is more precise than the conventional experimental procedure. We therefore aimed to describe the ISE on the (001) face of β-Sn single crystals by using the DSI technique and to determine the most suitable model for the estimation of true hardness to take the creep effect into account.

1.4. Creep behaviour

Among the different characteristics of the soft materials, creep behaviour is of great interest, mainly due to the need for attaining shape and mechanical properties. Several papers have addressed the possibility of gaining information on creep properties by the use of indentation or long time hardness tests [17–19]. The indentation creep test is a very convenient way by which various creep information can be obtained from a limited supply of material. In these tests, creep characteristics of materials are investigated through the indentation process, i.e. time-dependent plastic flow of the material just below the indenter. The indenter maintains its load over a period of time under well controlled conditions and the changes in the size of indentation are monitored during the experiment.

The DSI test can be also used to obtain creep data in cases where there is not enough material available to machine tensile or compression creep specimens or in cases where the creep properties of small amounts of materials need to be locally assessed. The indentation creep tests can be performed in two different ways by DSI. (i) The constant rate of loading (CRL) test is carry out at a prespecified loading rate that is varied from one indentation to another. This test can be defined as the time-dependent penetration of a hard indenter into the material under constant load and temperature. (ii) The other process is the loading rate change (LRC) or rate dependent test (RDT) [20], and the LRC tests are capable of determining the stress exponent, n, of different materials [21, 22].

2. Experimental procedure

β-Sn ingots used in this study were of 99.99% purity and were grown in a glass tube at the rate of 15 mm h^{-1} using a modified Bridgman method under 10^{-4} Torr pressure. Their orientations were determined by the Laue back-reflection method. The sample codes Sn_{1Y}, Sn_{2Y}, Sn_{3Y}, and Sn_{4Y} were used to refer to single crystals having 4°, 12°, 15°, and 20° angles with the growth direction [110], respectively. Surface damage was removed mechanically by grinding with 2400 and 4000 grit, and then polishing on 3 and 1 μm diamond lap wheels. To examine the surfaces, investigations were performed using a JEOL JSM-5400 scanning electron microscope (SEM). For SEM examinations, the samples were coated with a thin gold layer to avoid charging effects.

Hardness measurements of β-Sn single crystals were performed with a dynamic ultra-microhardness tester (Shimadzu, DUH-W201S), having a maximum penetration depth 10 μm and an indenter shift resolution of 1 nm, at room temperature. A load cell and displacement–voltage dilatometer (LVDT) were used to control the applied load and to measure the penetration depth of the indenter. The indentation experiments were performed on the (001) face for each specimen. For an easier interpretation of mechanical behaviour at various depths, the maximum load was changed at regular intervals, 10, 20, 30, 40, and 50 mN under a loading/unloading rate of 4.4130 mN s^{-1}, and the load was held at each maximum value for 300 s. For a particular load at least five indentation tests were conducted on the sample surface to increase the reliability of the experimental results.

3. Results and discussion

Figure 5 shows the representative applied indentation test load–penetration depth curves for different indentation test loads measured in the present study. For each record these curves were analysed using the aforementioned (Oliver–Pharr and Tang–Ngan) procedure. An SEM image of the residual impression produced by indentation is seen as an inset in figure 5. The elastic–plastic transition which can be seen in the figure is mentioned in the following section. Penetration depth dependences of H_d obtained for different oriented β-Sn single crystals are given in figure 6. The classical ISE was observed in all of the samples that were tested. The variation of H_d with applied indentation test load for each growth direction shows that H_d decreases with increasing applied indentation test load, and then reaches saturation at about 50 mN. The entire H_d profile consists of two regimes for all examined materials: load dependent (H_{LD}) and load independent (H_{LI}).

As can be seen from figures 3–5, the nose effect disappears with brief load holds prior to unloading the examined materials. Therefore, the reduced modulus can no longer be calculated from equation (2). Therefore, the reduced modulus and dynamic hardness of the materials are calculated by the Feng–Ngan method [4] and the Tang–Ngan [10] procedure. These procedures involve the correction of both h_c and S_e for the creep effect.

3.1. Analysis of the ISE behaviour

The ISE has been examined extensively for different kinds of materials. Many attempts have been made to clarify the load dependence and to develop more or less realistic models to interpret hardness tests [23–27].

Firstly we used the empirical equation for describing the ISE in the Meyer's law [28, 29], which uses a correlation technique between the applied indentation test load and the resultant

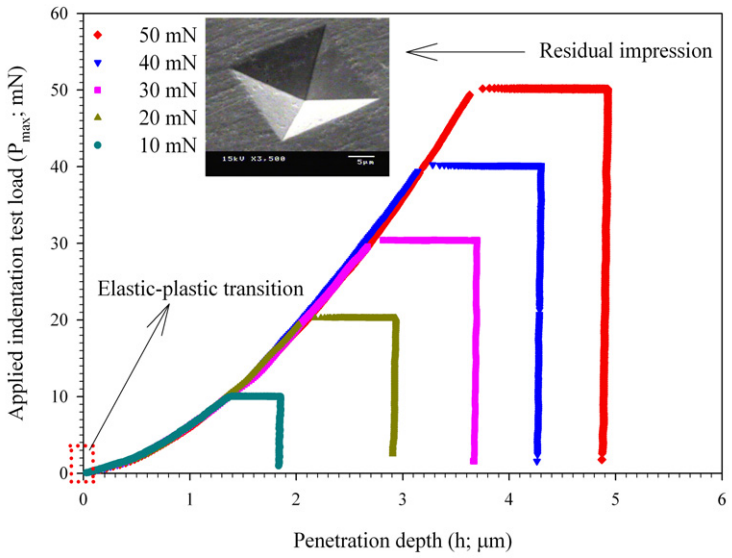

Figure 5. Typical applied indentation test load–penetration depth curves of indentation tests of β-Sn single crystals (holding time 300 s).

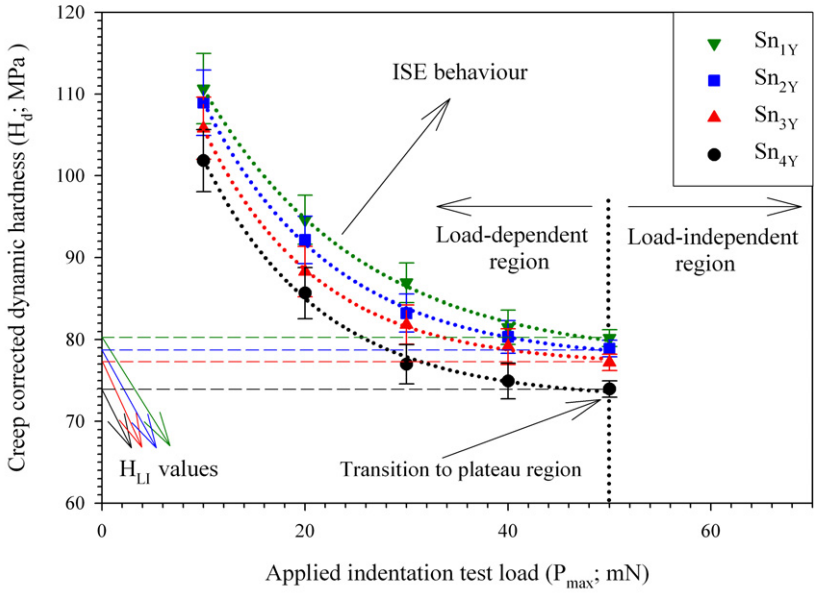

Figure 6. Creep corrected dynamic hardness variation as a function of applied indentation test load for β-Sn single crystals.

indentation size using a simple power law,

$$P_{\max} = Ch_c^n \tag{7}$$

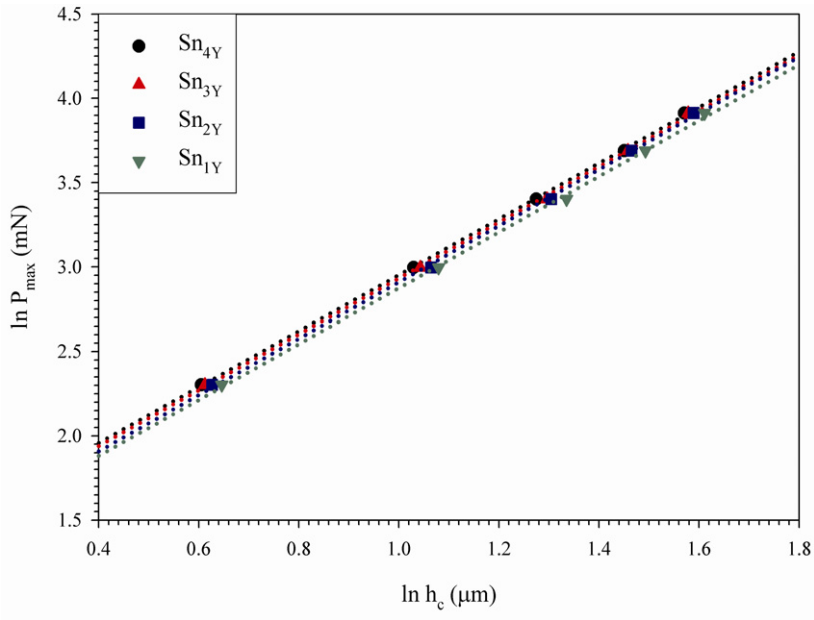

Figure 7. Plots of ln P_{max} versus ln h_c according to the Meyer's law.

Table 1. Regression analysis results of experimental data according to equation (7).

Sample code	n	C (mN μm^{-n})	r^2
Sn_{1Y}	1.655	0.197	0.998
Sn_{2Y}	1.669	0.214	0.999
Sn_{3Y}	1.655	0.244	0.999
Sn_{4Y}	1.657	0.257	0.999

where C and n are constants derived directly from curve fitting of the experimental data. In particular, the exponent n, sometimes referred to as the Meyer index, is usually considered as a measure of ISE. Compared to the definition of the apparent hardness (equation (7)), no ISE would be observed for $n = 2$.

The indentation data for the examined materials in the present study were plotted in figure 7. The data showed a linear relationship, implying that the traditional Meyer's law was suitable for describing the indentation data. Through linear regression analyses, the best-fit values of the parameters C and n were obtained and the results were summarized in table 1. The calculated n values pointing out the decrease of dynamic hardness with the increasing applied indentation test load are in agreement with an ISE (figure 6). However, several studies [15, 16, 23, 29] have reported that the classic Meyer law is insufficient to describe the origin of the ISE. Therefore, a new method is needed to achieve a basic understanding of the ISE.

The experimental data on the dependence of H_d on applied peak indentation test load can be explained by the Hays–Kendall approach [30]. They proposed that there exists a minimum applied test load W (test specimen resistance) necessary to initiate plastic deformation, below which only elastic deformation occurs. On the basis of the hypothesis equation (7) is modified

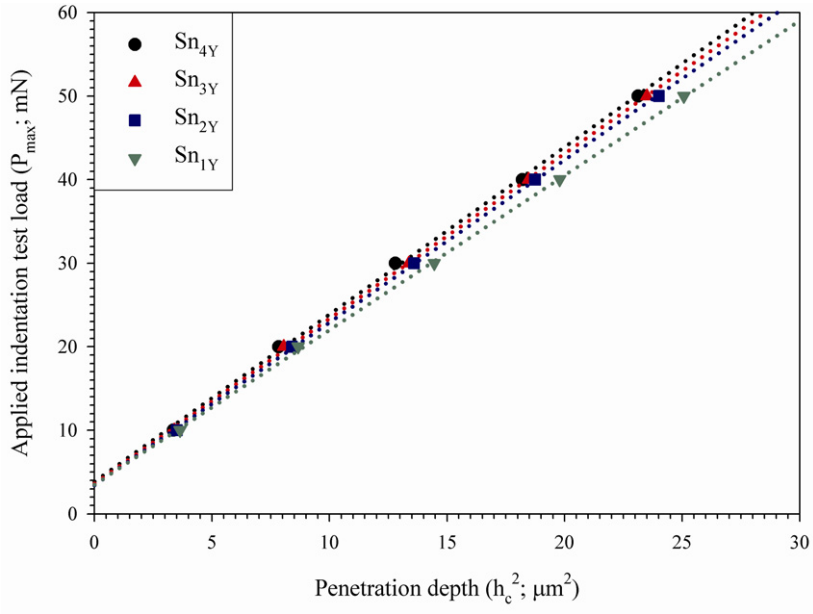

Figure 8. Plots of P_{max} versus h_c^2 according to the Hays–Kendall model.

to

$$P_{\text{effective}} = P_{\max} - W = C_1 h_c^2, \tag{8}$$

where C_1 is a constant independent of the test load and $(P_{\max} - W)$ is an effective indentation load. Replacing $P_{\max}$ in equation (5) by $(P_{\max} - W)$, one gets an equation to calculate the load-independent (or true) hardness as follows:

$$H_{\text{HK}} = \frac{(P_{\max} - W)}{26.43 h_c^2} = 0.0378 \frac{(P_{\max} - W)}{h_c^2} = 0.0378 C_1. \tag{9}$$

From equation (8), a plot of $P_{\max}$ versus h_c^2 would yield a straight line, where W and C_1 parameters can easily be calculated from the intersection point and slope of the curve, respectively. Such a plot for β-Sn single crystals having different crystal growth directions considered in the present study is shown in figure 8. From the figure, the W values are 3.486, 3.421, 3.616, and 3.852 mN for Sn_{1Y}, Sn_{2Y}, Sn_{3Y}, and Sn_{4Y}, respectively. The correlation coefficients for all materials, r^2, are 0.999, implying that equation (8) provides a satisfactory description of the indentation data for the examined test materials. On the other hand, further from the magnified applied indentation test load–penetration depth (from figure 5) curve shown in figure 9, it was found that, with the indentation depth smaller than 0.3 μm, the loading curve rather matched the elastic unloading curve in accordance with the 'Hertzian elastic relation' [31], revealing the purely elastic response of the β-Sn single crystals without any plastic deformation under extremely small strain. As the applied indentation test load exceeded 1.1 mN, the curve deviated from the 'Hertzian response', after which it was expected that the stress intensity at the indenter tip had accumulated to the critical shear stress for the plastic deformation (yielding) of the β-Sn single crystals. Therefore, the minimum load required for initiating the permanent deformation predicted by the Hays–Kendall approach is too large to be accepted, invalidating the applicability of this approach in analysing the ISE. As a result,

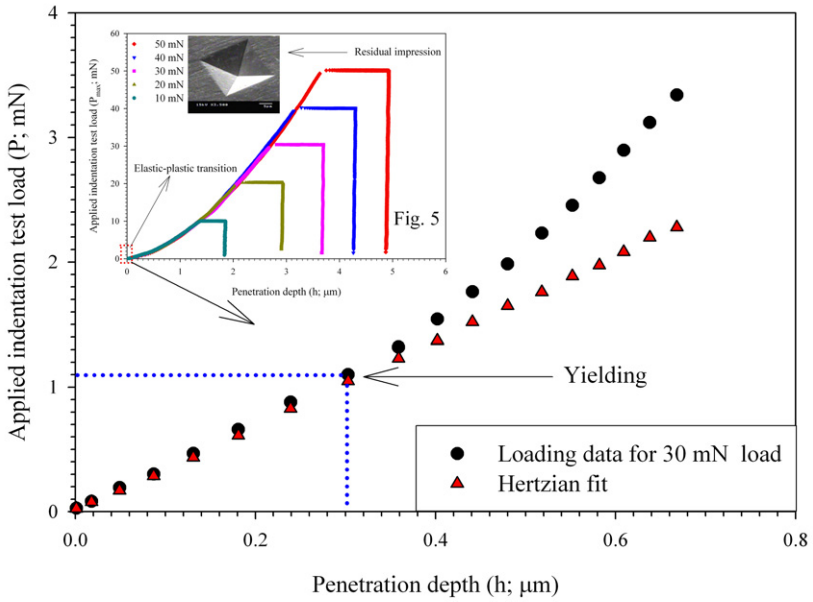

Figure 9. Magnified applied indentation test load–penetration depth curve for 30 mN load.

one can conclude that the Hays–Kendall approach is not appropriate for describing the ISE behaviour observed in β-Sn single crystals.

Recently, Li and Bradt [32] have tried to explain the ISE with the aid of their 'proportional specimen resistance' (PSR) model. According to the PSR model, there are two factors responsible for the decrease in dynamic hardness with increase in load. In this model, the applied indentation test load, $P_{\max}$, is related to the contact depth, h_c, as follows:

$$P_{\max}/h_c = a_1 + a_2 h_c, \tag{10}$$

where the parameters a_1 and a_2 are constants for a given material. According to the analysis by Li and Bradt, the parameters a_1 and a_2 can be related to the elastic and the plastic properties of the test material, respectively. In particular, a_2 is suggested to be a measure of the so-called '*true hardness*, H_{PSR}'. For the indentation test with a Vickers indenter, H_{PSR} can be determined directly from a_2 with

$$H_{PSR} = \frac{(P_{\max} - a_1 h_c)}{26.43 h_c^2} = \frac{a_2}{26.43}. \tag{11}$$

According to equation (10), a plot of $P_{\max}/h_c$ versus h_c should yield a straight line, where a_1 and a_2 parameters can easily be calculated from the intersection point and slope of the curve, respectively (figure 10). The estimated best-fit values of a_1 and a_2 parameters and corresponding H_{PSR} values are listed in table 2.

The PSR model may be considered to be a modified form of the Hays–Kendall approach to the ISE. The model treats the specimen's resistance to permanent deformation as a function of indentation size, rather than constant (i.e. $W = a_1 h_c$) [32]. Li *et al* concluded that this model might provide a satisfactory explanation for the origin of ISE in hardness tests for different kinds of materials. On the other hand, Quinn and Quinn [33] have recently examined

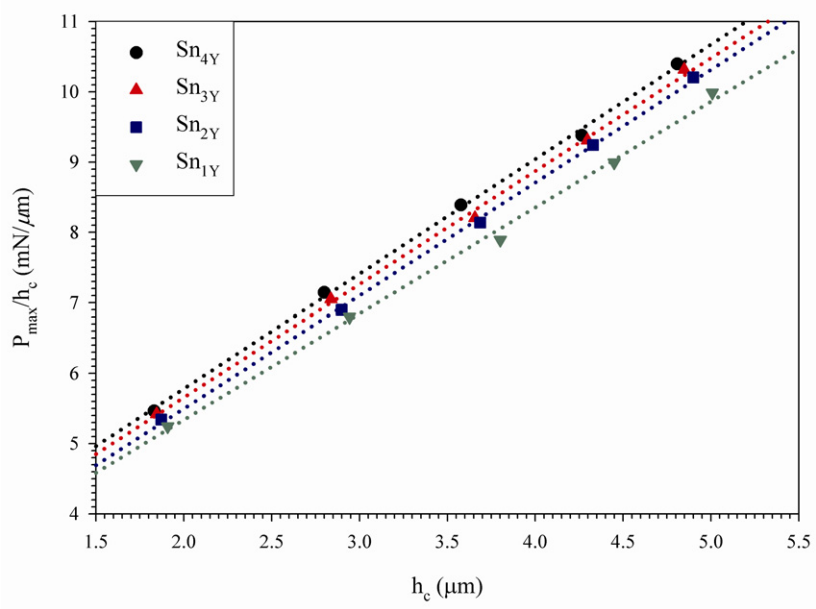

Figure 10. Plots of P_{max}/h_c versus h_c according to the PSR model.

Table 2. Best-fit results of PSR model according to equation (10).

Sample code	a_1 (mN μm^{-1})	a_2 (mN μm^{-2})	H_{PSR} (MPa)	H_{LI} (MPa)
Sn_{1Y}	2.321	1.505	56.942	80.181
Sn_{2Y}	2.282	1.606	60.764	78.896
Sn_{3Y}	2.435	1.608	60.839	77.217
Sn_{4Y}	2.515	1.631	61.710	73.940

the variation of Vickers hardness with applied indentation test load for a variety of ceramic materials. These researchers observed that such a hardness–load curve exhibited a distinct transition to a plateau of constant hardness and claimed that such a curve corresponded to the intrinsic hardness value of the materials. In the present study, figure 2 shows the transition point (about 50 mN) and corresponding load-independent (H_{LI}) hardness values, 80.181, 78.896, 77.217, and 73.940 MPa for Sn_{1Y}, Sn_{2Y}, Sn_{3Y}, and Sn_{4Y}, respectively. In the light of the Quinn and Quinn approximation, the load-independent hardness value (H_{PSR}) calculated with the PSR model (table 2) is far from the intrinsic hardness value for β-Sn single crystals. Therefore, it may be suggested that the PSR model may also be insufficient to explain the ISE behaviour of the present β-Sn single crystals.

According to the PSR model, when $h_c = 0$, the test specimen resistance ($W = a_1 h_c$) becomes zero. This implies that the minimum applied load needed to produce permanent deformation is zero for a given material. However, Gong *et al* reported that this definition is unreasonable [23]. The test specimen subjected to surface machining and polishing processes can be considered as a compressed spring rather than stress free material. Hence, they suggested the modified form of the PSR model, as given in equation (12).

$$P_{max} = a_0 + a_1 h_c + a_2 h_c^2, \tag{12}$$

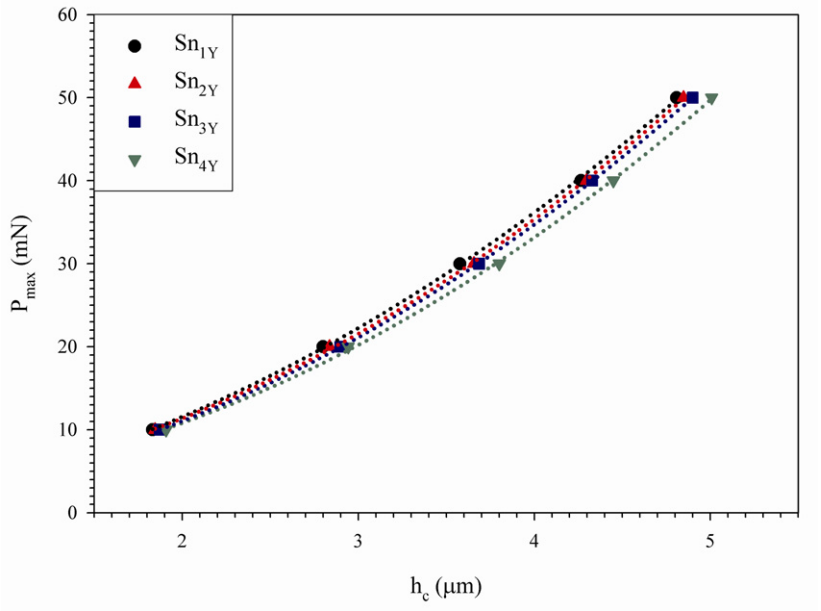

Figure 11. Plots of P_{max} versus h_c according to the MPSR model.

Table 3. Best-fit results of MPSR model according to equation (12).

Sample code	a_0 (mN)	a_1 (mN μm^{-1})	a_2 (mN μm^{-2})	H_{MPSR} (MPa)	H_{LI} (MPa)
Sn_{1Y}	2.752	0.465	1.783	67.461	80.181
Sn_{2Y}	1.568	1.193	1.772	67.045	78.896
Sn_{3Y}	1.719	1.240	1.791	67.763	77.217
Sn_{4Y}	−0.114	2.608	1.614	61.066	73.940

where a_0 is a constant related to the residual surface stresses associated with the surface machining and polishing and a_1 and a_2 are the same parameters as given in equation (10).

Similar to the PSR model, the true hardness of the modified PSR model, H_{MPSR}, can be determined directly from a_2 with

$$H_{MPSR} = \frac{(P_{max} - a_0 - a_1 h_c)}{26.43 h_c^2} = \frac{a_2}{26.43}. \tag{13}$$

Best-fit values of a_0, a_1 and a_2 parameters estimated from figure 11 and corresponding H_{MPSR} values are listed in table 3. When we examine table 3 together with table 2, it can be seen that the H_{MPSR} values (table 3) are closer to plateau values than estimated hardness results (H_{PSR}) by the PSR model (table 2). Therefore, the MPSR model seems to be more reasonable than the PSR according to Quinn and Quinn [33]. On the other hand, the a_0 parameter given in equation (12) points out the same physical meaning as the W stated in the Hays–Kendall model.

Evidently, the a_0 value is still too high to characterize the load required to initiate permanent deformation of the surface (figure 9). In the literature, Peng *et al* [34] reported a similar conflict for the a_0 parameter. One may therefore recommend that the modified PSR model may also be inadequate in determination of the threshold load like the Hays–Kendall model.

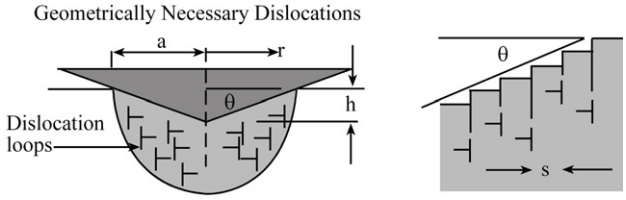

Figure 12. Schematic illustration of GND loops [27].

It is accepted that a_0 in equation (12) is a specimen constant, rather than a material constant. This parameter depends not only on the materials properties but also on the surface finishing process used in the preparation of the specimens. The relatively smaller values of a_0 in table 3 seem to be reasonable estimates of the residual surface stresses for the β-Sn test specimens, which have been subjected to a careful polishing after machining. On the other hand, the parameter a_1 varies from one crystal growth direction to another. This is not surprising, since a_1 indicates the surface contribution to the indentation hardness. The differences in the a_1 values are in fact related to real differences in the surface contributions to the indentation hardness for different crystal growth directions [15, 16]. The a_2 and H_{MPSR} values (except for $\mathrm{Sn_{3Y}}$) decrease with decreasing deviation from the [110] crystal growth direction.

The other model has been developed by Nix and Gao [27], who proposed a mechanism based theory of strain gradient plasticity (MSG) responsible for the ISE. The MSG theory assumes that the indentation is accommodated by circular loops of geometrically necessary dislocations (GNDs) with Burgers vectors normal to the plane surface (figure 12). The model combines the Taylor relation [35], the Mises flow rule, and the Tabor relation [36] to obtain the following characteristic expression for the depth dependence of hardness:

$$\frac{H}{H_0} = \sqrt{1 + \frac{h^*}{h}}. \tag{14}$$

H is the nominal hardness for a given depth; h and h^* are characteristic depths which depend on the shape of the indenter and the material. Finally, H_0 can be defined as the hardness that would arise from the statistically stored dislocations alone, or equivalently the hardness obtained in the limit for an infinite depth (size independent hardness).

In figure 13, the square of the dynamic hardness value obtained in the indentation tests is plotted as a function of the reciprocal of the indentation depth. There is a linear relationship between H^2 and $1/h$, in agreement with equation (14). This means that the dynamic hardness decreases due to the indentation size effect. The values of H_0 and h^* can easily be determined from the intersection point and the slope of the curve, respectively. Then the relationship between $(H/H_0)^2$ and $1/h$ is shown in figure 14. It is almost linear and also consistent well with reference [27].

The Nix and Gao model can be used to determine the size-independent (load-independent) dynamic hardness values, H_{NG}, of β-Sn single crystals. The obtained values were 46.626, 50.917, 50.427, and 52.710 MPa for $\mathrm{Sn_{1Y}}$, $\mathrm{Sn_{2Y}}$, $\mathrm{Sn_{3Y}}$, and $\mathrm{Sn_{4Y}}$, respectively. H_{NG} values (except for $\mathrm{Sn_{3Y}}$) increase with decreasing deviation from the [110] crystal growth direction. We utilized the PSR (table 2), MPSR (table 3), and Nix–Gao methods to determine the load independent hardness values of β-Sn single crystals. It can be seen that the H_{MPSR} values are closer to plateau values than those of the PSR and Nix–Gao methods.

S_{u}, S_{e}, and h_{c} were determined using the OP method and the Tang–Ngan procedure, and then, using the DSI data, the reduced modulus was calculated. Creep corrected dynamic

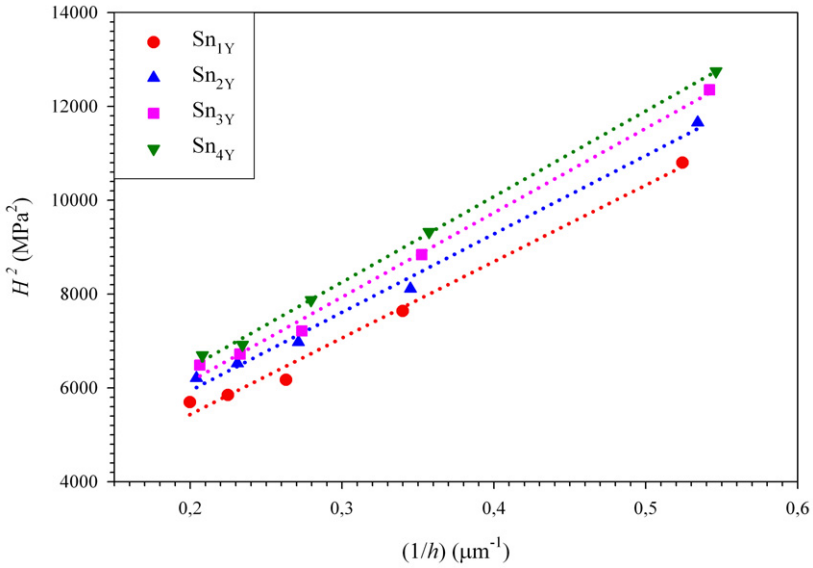

Figure 13. The relationship between H^2 and $1/h$ of β-Sn single crystals.

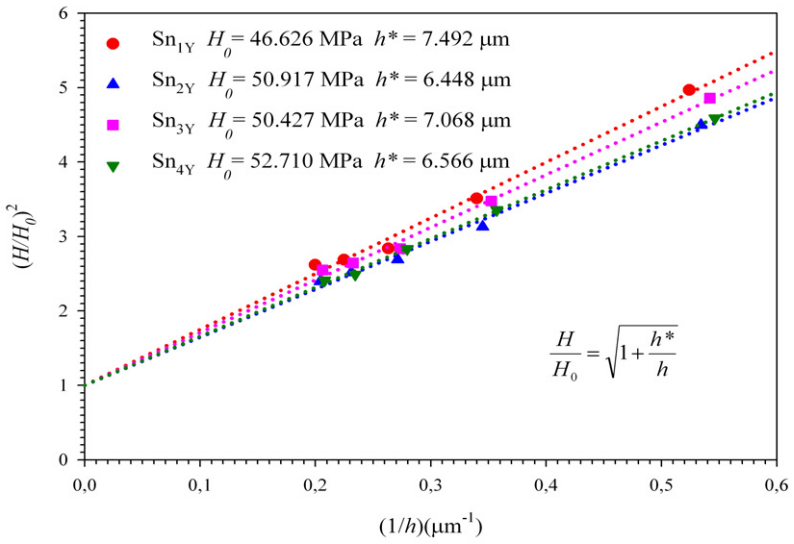

Figure 14. Application of Nix and Gao model to β-Sn single crystals.

hardness and reduced modulus as a function of the applied indentation test loads are shown in figures 15(a)–(d). The dynamic hardness and reduced modulus for all crystal growth directions remained constant at increasing applied indentation test loads, as shown in the figures. The slight increase in dynamic hardness (ISE) and decrease in reduced modulus at smaller indentation test loads (reverse indentation size effect; RISE) were due to the indenter tip roundness and the surface oxidation of the examined materials [2]. Another influence may be mechanical polishing before the indentation tests of these crystals. Detailed explanations were

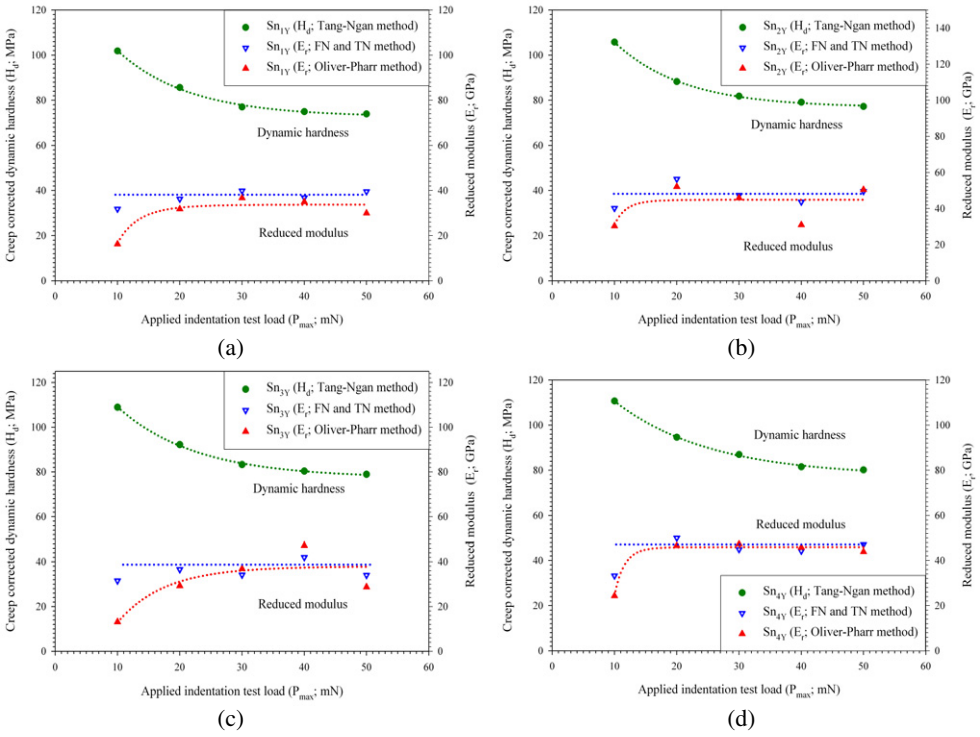

Figure 15. (a) Creep corrected dynamic hardness and reduced modulus as a function of the applied indentation test load for Sn_{1Y}. (b) Creep corrected dynamic hardness and reduced modulus as a function of the applied indentation test load for Sn_{2Y}. (c) Creep corrected dynamic hardness and reduced modulus as a function of the applied indentation test load for Sn_{3Y}. (d) Creep corrected dynamic hardness and reduced modulus as a function of the applied indentation test load for Sn_{4Y}.

given in our earlier study [16]. Texture is another source of deviation of reduced modulus. These materials are highly anisotropic, and because of this it is not clear to what value the measured modulus should be compared. On the other hand, it can be argued that the most appropriate modulus is that in the direction of testing, since the elastic displacements are primarily in this direction. On the other hand, since the formation of the contact impression involves deformation in many directions, it can be argued that the measured modulus should be some average quantity [1]. Similarly, Vlassak and Nix [37, 38] investigated the reduced modulus of cubic crystals at different orientations by indentation. For Cu and β-brass, along {1 1 1} the indentation modulus was found to be 10–25% larger than along {1 0 0}.

On the other hand, the creep corrected reduced modulus remains more or less constant over the entire range of load. The values are 39.000, 44.100, 39.500, and 43.500 GPa for Sn_{1Y}, Sn_{2Y}, Sn_{3Y}, and Sn_{4Y}, respectively. Our results are comparable with that of Deng *et al*, who obtained the modulus value of pure Sn as 46.9 ± 2.7 GPa using nanoindentation tests [39].

4. Concluding remarks

This paper presents the results of dynamic hardness and reduced modulus on β-Sn single crystals at various loads using creep curves. The dynamic hardness and reduced modulus of the crystals were deduced both the OP method and the Tang–Ngan procedure. The conclusions arising from the work are as follows.

(1) The reduced modulus calculated using the Oliver–Pharr method becomes negative due to the occurrence of a nose in the unloading applied indentation load–penetration depth curve. The nose effect disappears with brief load holds prior to unloading. We therefore calculated H_d and E_r using the OP method and the Tang–Ngan procedure.
(2) In the analysis of the ISE, the classical Meyer's law may yield a good fit for the measured indentation data. However, there is no useful information on the origin of the observed ISE for β-Sn single crystals.
(3) The PSR model can be used to analyse the ISE observed in β-Sn single crystals but it failed in analysing the reserved ISE behaviour observed in the examined materials, since the load-independent hardness values are below the plateau region.
(4) The minimum load required for initiating the permanent deformation predicted by the Hays–Kendall approach is too large to be accepted, invalidating the applicability of this approach in analysing the ISE.
(5) The calculated load-independent hardness values by the modified PSR model are more useful than those obtained by the PSR and Nix–Gao models. However, the modified PSR model may also be insufficient to determine the threshold load to produce initiation of permanent deformation.
(6) The Nix–Gao model can be used to analyse the ISE. However, the load-independent hardness values are below the plateau region, the same as the PSR model.
(7) Compared to the Oliver–Pharr method both the Feng–Ngan and Tang–Ngan methods together seem to work well for H_d and E_r calculation of β-Sn single crystals from the creep curves. Calculated E_r values from the latter procedures are consistent with the literature [39].

Acknowledgments

The authors would like to acknowledge the financial support (project no 2003K120510) by the Turkish State Planning Organization (DPT). The financial support from the Turkish Scientific and Technical Research Institute (TUBİTAK) Münir Birsel charity is also gratefully acknowledged. The authors also thank Dr B Düzgün from Atatürk University, Turkey, for supplying the sample.

References

[1] Oliver W C and Pharr G M 1992 *J. Mater. Res.* **7** 1564
[2] Li X and Bhushan B 2002 *Mater. Charact.* **48** 11
[3] Elmustafa A A and Stone D 2002 *Acta Mater.* **50** 3641
[4] Feng G and Ngan A H W 2002 *J. Mater. Res.* **17** 660
[5] Chudoba T and Richter F 2001 *Surf. Coat. Technol.* **148** 191
[6] Feng G and Ngan A H W 2001 *Fundementals of Nanoindentation and Nanotribology II* (*Mater. Res. Soc. Symp. Proc.* vol 649) ed S P Baker, R F Cook, S G Corcoran and N R Moody (Warrendale, PA: Material Research Society) p Q7.1.1
[7] Radok J R M 1957 *Q. Appl. Math.* **15** 198
[8] Lee E H and Radok J R M 1960 *J. Appl. Mech.* **27** 438
[9] Ting T C T 1966 *J. Appl. Mech.* **33** 845
[10] Tang B and Ngan A H W 2003 *J. Mater. Res.* **18** 1141
[11] Suresh S, Nieh T G and Choi B W 1999 *Scr. Mater.* **41** 951
[12] Kiely J D, Jarausch K F, Houston J E and Russell P E 1999 *J. Mater. Res.* **14** 2219
[13] Zimmerman J A, Kelchner C L, Klein P A, Hamilton J C and Foiles S M 2001 *Phys. Rev. Lett.* **87** 165507
[14] Li J, Van Vliet K J, Zhu T, Yip S and Suresh S 2002 *Nature* **418** 307

[15] Sahin O 2006 The relationship between crystal orientation and some mechanical properties of β-Sn single crystals *PhD Thesis* Suleyman Demirel University, unpublished
[16] Sahin O, Uzun O, Kolemen U, Düzgün B and Uçar N 2005 *Chin. Phys. Lett.* **22** 3137
[17] Mahmudi R, Roumina R and Raeisinia B 2004 *Mater. Sci. Eng.* A **382** 15
[18] Fujiwara M and Otsuka M 2001 *Mater. Sci. Eng.* A **319–321** 929
[19] Feng G and Ngan A H W 2001 *Scr. Mater.* **45** 971
[20] Wen S P, Zeng F, Gao Y and Pan F 2006 *Scr. Mater.* **55** 187
[21] Mahmudi R and Bazzaz A R 2005 *Mater. Lett.* **59** 1705
[22] Sahin O and Uçar N 2006 *Chin. Phys. Lett.* **23** 3037
[23] Gong J, Wu J and Guan Z 1999 *J. Eur. Ceram. Soc.* **19** 2625
[24] Gong J, Zhao Z, Guan Z and Miao H 2000 *J. Eur. Ceram. Soc.* **20** 1895
[25] Sangwall K, Surowska B and Blaziak P 2002 *Mater. Chem. Phys.* **77** 511
[26] Sangwall K, Surowska B and Blaziak P 2003 *Mater. Chem. Phys.* **80** 428
[27] Nix W D and Gao H 1998 *J. Mech. Phys. Solids* **46** 411
[28] Meyer E 1908 *Phys. Z.* **9** 66
[29] Kölemen U 2006 *J. Alloys Compounds* **425** 429
[30] Hays C and Kendall E G 1973 *Metall* **6** 275
[31] Fischer-Cripps A C 2004 *Nanoindentation* (New York: Springer) p 71
[32] Li H and Bradt R C 1993 *J. Mater. Sci.* **28** 917
[33] Quinn J B and Quinn G D 1997 *J. Mater. Sci.* **32** 4331
[34] Peng Z, Gong J and Miao H 2004 *J. Eur. Ceram. Soc.* **24** 2193
[35] Ashby M F 1970 *Phil. Mag.* **21** 399
[36] Tabor D 1951 *The Hardness of Metals* (Oxford: Clarendon) p 105
[37] Vlassak J J and Nix W D 1994 *J. Mech. Phys. Solids* **42** 1223
[38] Vlassak J J and Nix W D 1993 *Phil. Mag.* A **67** 1045
[39] Deng X, Chawla N, Chawla K K and Koopmen M 2004 *Acta Mater.* **52** 4291